Communication

Reliability Analysis of A MEMS Flow Sensor with Accelerated Degradation Test

Qiaoqiao Kang , Yuzhe Lin , Jifang Tao *

Posted Date: 19 September 2023

doi: 10.20944/preprints202309.1271.v1

Keywords: Flow sensor; Accelerated degradation testing; Reliability

Communication

Reliability Analysis of a MEMS Flow Sensor with Accelerated Degradation Test

Qiaoqiao Kang [1], Yuzhe Lin [2] and Jifang Tao [2,*]

[1] Key Laboratory of Laser & Infrared System Ministry of Education, Shandong University, Qingdao 266237, China; 202020457@mail.sdu.edu.cn

[2] School of Information Science and Engineering, Shandong University, Qingdao 266237, China; Linyz@sdu.edu.cn

* Correspondence: taojf@sdu.edu.cn;

Abstract: With the wide application of flow sensor, their reliability under extreme conditions has been concerned in recent years. The reliability of a Micro Electro Mechanical Systems flow sensor under temperature (T_s) is researched in this paper. Firstly, the Step-stress accelerated degradation test is designed. Because this flow sensor consists flow sensor chip and signal processing system, the accelerated degradation testing is implemented, respectively. While the results show that the biggest drift is 3.15% for flow sensor chips with 150℃ conditions, and 32.91% for this flowmeter. By analysis, it could be found that the attenuation of the signal processing system is significant to the degeneration of this flowmeter. The minimum drift of the signal processing system accounts for 82.01% of this flowmeter. Secondly, using the Coffin-Manson model, the relationship between cycle-index and T_s is established. And the lifetime with different T_s is estimated by the Arrhenius model. In addition, the Weibull distribution is applied to evaluate the lifetime distribution. Finally, the reliability function of the Weibull distribution is demonstrated, and the survival rate within one year is 87.69% with 85℃ conditions. Thus, by the application of accelerated degradation testing, the acquired results are innovative and original. This research illustrates the reliability research, which provides a relational database for the application of this flow sensor.

Keywords: flow sensor; accelerated degradation testing; reliability

1. Introduction

Flow sensor has been widely used in metrology and industry as a fundamental device [1–3]. It has received continuous attention and in-depth research of worldwide researchers with Micro Electro Mechanical Systems (MEMS) technology [4–6]. In this paper, this flow sensor has consisted of MEMS sensor chip and signal processing system (SPS), which requires analog sub-systems such as amplifiers, comparators, filters, digital-analog and analog-digital converters. As is known, the MEMS flow sensor has the advantages of low cost and high sensitivity. Moreover, the application of a MEMS flow sensor is good industrialization prospect. With the progress of science and technology, the efficient and intelligent flow sensor is often used in a high-temperature or high-humidity environments. [7–10]. Especially with the continuous development of MEMS Flow sensor, the application field is more and more extensive. Unfortunately, the high performance and integrated functions get superabundant attention, and the reliability tends to be forgotten. However, the MEMS sensor chip, as the core of the whole flow sensor system, suffers from degradation and reduced reliability, which constitutes a major hazard to the safety performance of the system. Thus, the reliability of flow sensor under extreme conditions has been paid much more attention in recent years [11–19]. In addition, the reliability of electronic devices system, especially on their performance with concerning for SPS had been reported very little frequently, even though the fact that the SPS was one of the weakest components in the entire system [20–22]. Consequently, ensuring the reliability of flow sensor under

Preprints (www.preprints.org) | NOT PEER-REVIEWED | Posted: 19 September 2023 doi:10.20944/preprints202309.1271.v1

extreme conditions cannot be ignored for their future operating characteristic and commercialization. Accelerated degradation testing (ADT) has been widely applied as an efficient strategy to obtain the reliability (life) information of the assets in a shorter-than-normal period time by exposing the assets to higher-than-normal stresses [9]. The ADT is a good way to study the devices under extreme conditions, especially Step-stress accelerated degradation test (SSADT) can set different temperatures during a finite test period time [10–15].

In this paper, a MEMS flow sensor lifetime and reliability is reported. Based on the SSADT of temperature stress (T_s), the influences of T_s on MEMS sensor chips, SPS, and entire flow sensor are discussed, respectively. The acquired results are innovative and original, and the lifetime of MEMS flow sensor is estimated. Using Coffin-Manson illustrated the relationship between cycle-index and T_s. And lifetime is estimated with the Arrhenius model. Finally, the Weibull distribution (WD) is applied to analyze the lifetime distribution. This paper is organized as follows. Section 2 elaborates on the experiment steps and methods. The experiment results of SSADT are obtained and discussed in Section 3. Section 4 estimates the lifetime distribution and predicts reliability with WD.

2. Materials and Methods

As the Figure 1 shows, the flow sensor consists of a MEMS flow sensor chip and the SPS. Meanwhile, the MEMS flow sensor includes three parts: Micro-heater, sensitive area and a silicon substrate. By the way, the polysilicon resistor was simultaneously used as a heating structure (Micro-heater) and sense structure (up/down-downstream thermopile).

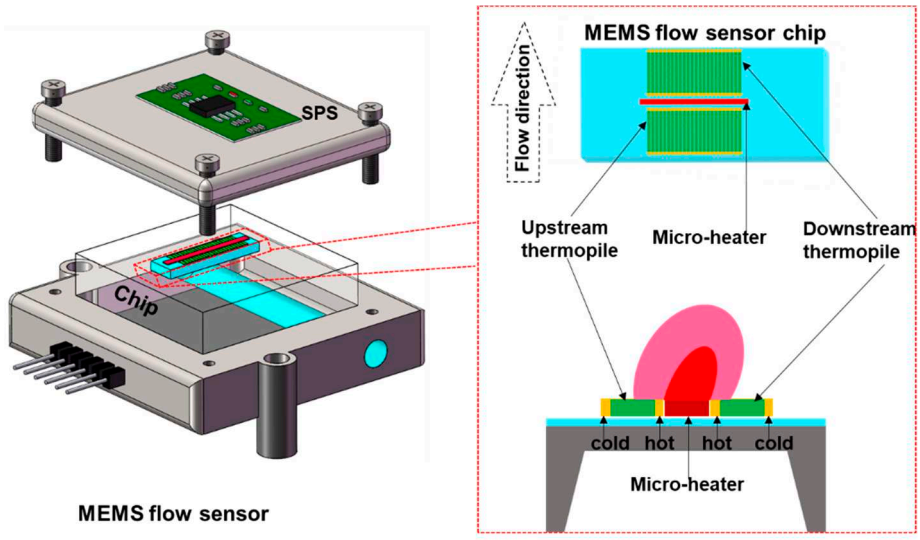

Figure 1. MEMS Flow sensor.

For this MEMS flow sensor, the physical principles of thermoelectric generation are based on Seebeck effect. As shown in Equation (1), Seebeck coefficient is an important actor for this MEMS sensing chip.

$$\alpha_{ab} = \frac{d\Theta_{ab}}{dT} \quad (\mu V/K) \tag{1}$$

α_{ab} is coefficient of Seebeck. Θ_{ab} is potential (electric) force of Seebeck. T is temperature of Micro-heater. When voltage is applied to the Micro-heater, the Micro-heater will generate heat to warm up the surroundings. The hot junctions of two thermopiles are heated. Then generate initial thermoelectric voltage. When there was air flow, the thermal field distribution is changed, leading to the initial voltage of the thermopile be changed accordingly [23–27].

Before ADT, the resistance of Micro-heater (RHG) and the resistance of the up-downstream thermopile (RUG, RDG) were test separately. The average value (AVG) of output voltage at 100 sccm and 500 sccm were shown in Table 1. And the resistors value was acquired too, as shown in Table 2. On the other hand, the operation voltage is 3.3V for Flow sensor. As the Finite element simulation

Preprints (www.preprints.org) | NOT PEER-REVIEWED | Posted: 19 September 2023 doi:10.20944/preprints202309.1271.v1

results shown in Figure 2 (a), the maximum temperature is 184℃, but the SPS cannot withstand for long periods of time. Thus, to complete the accelerated experimental data in a short time and obtain effective experimental phenomena and data. SSADT with the 85℃-120℃-150℃ T_s is performed.

Table 1. Repeatability and Consistency of Flow sensor

Flow	Index	#1	#2	#3	#4	#5	#6
100 sccm	Avg(V)	1.868	1.873	1.856	1.863	1.844	1.867
500 sccm	Avg(V)	4.801	4.856	4.885	4.894	4.872	4.893

Table 2. Repeatability and Consistency of Flow sensor chip

	Index	#1	#2	#3	#4	#5	#6
RUG	Avg(KΩ)	119.7	118.1	122.5	121.1	121.3	115.8
RDG	Avg(KΩ)	116.5	122.2	114.7	120.2	122.8	120.2
RHG	Avg(Ω)	704.3	703.6	704.5	705.3	704.6	703.7

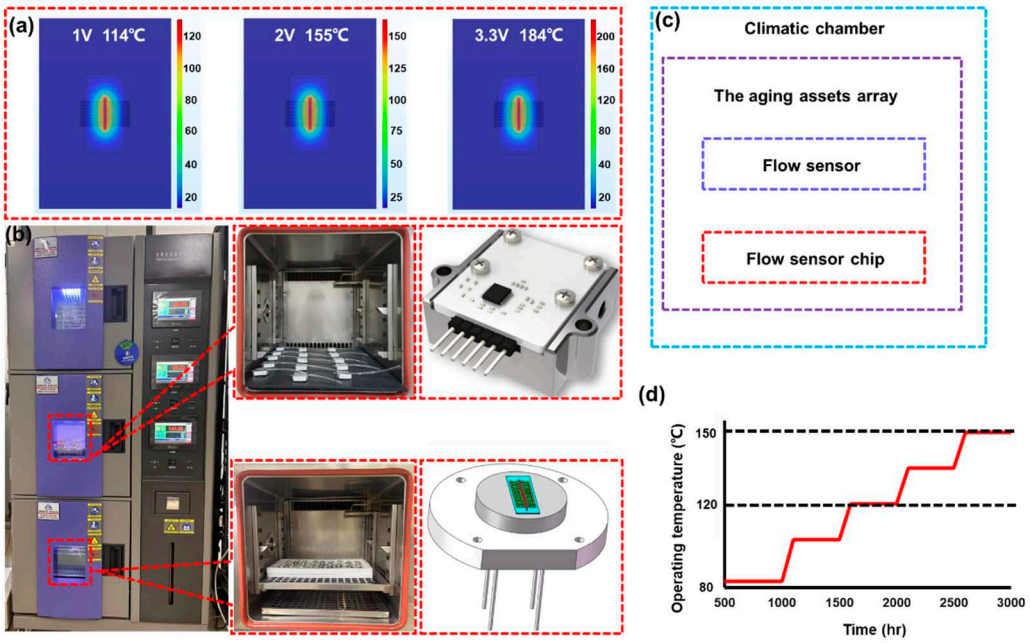

Figure 2. Experiment facilities. (**a**) Temperature distribution with voltage by Finite element simulation; (**b**). Climatic chamber and tested assets; (**c**). ADT process; (**d**). Example of testing cycle for ADT.

As showed in Figure 2, the ADT is carried out on the flow sensor chip and flow sensor simultaneously, which is set up in climatic chamber. Figure 2 (b)-(d) show the assets have been put into the climatic chamber. The test period for every temperature gradient of SSADT is 500 hours, each cycle takes 3000 hours, as shown in Figure 2 (d).

Preprints (www.preprints.org) | NOT PEER-REVIEWED | Posted: 19 September 2023 doi:10.20944/preprints202309.1271.v1

3. ADT Description

3.1. ADT Results

As is shown in Figure 1, considering the structure of this MEMS flow sensor, the output voltage changes as the drifts of characteristic parameters for the flow sensor, and the changes of resistors is acquired as the drifts of characteristic parameters for the sensor chip. The results of drifts of the characteristic parameters were presented. Specifically, the resistance drifts of 85℃, 120℃, and 150℃ T_s of RHG, RDG, and RUG were tested. As shown in Figure 3 (a)-(c), where ΔR is the changes of resistor and R_0 is the initial resistor. After 3000 hours aging, the biggest drift of 85℃, 120℃, and 150℃ were 1.35%, 2.09%, and 3.15%. It could be found that with the increases of T_s, the $\Delta R / R_0$ was more obvious.

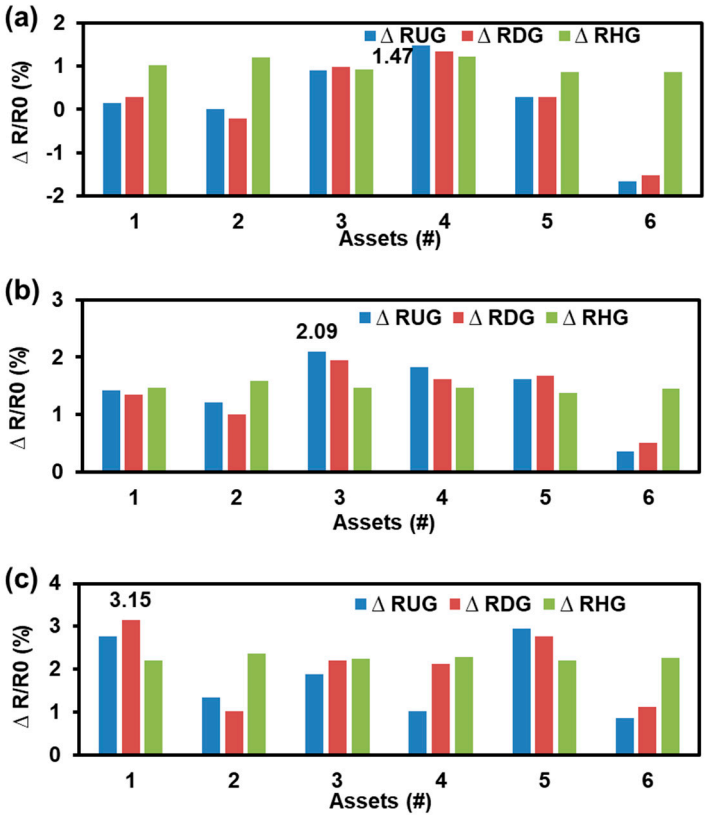

Figure 3. The ADT results of flow sensor chip with SSADT. (**a**) The maximum drift was 1.45% for 85℃; (**b**). The maximum drift was 2.09% for 120℃; (**c**). The maximum drift was 3.15% for 150℃.

On the other hand, the drift of this flow sensor was acquired too. V_0 is the initial output voltage of various flow rates and ΔV corresponds to changes. Comparing Figure 4 (a)-(c), it could be found the higher T_s the stronger attenuation. In addition, the attenuation of the larger flow rate was enhanced obviously. The biggest drift was -32.91% at 500 sccm with 150℃.

Preprints (www.preprints.org) | NOT PEER-REVIEWED | Posted: 19 September 2023 doi:10.20944/preprints202309.1271.v1

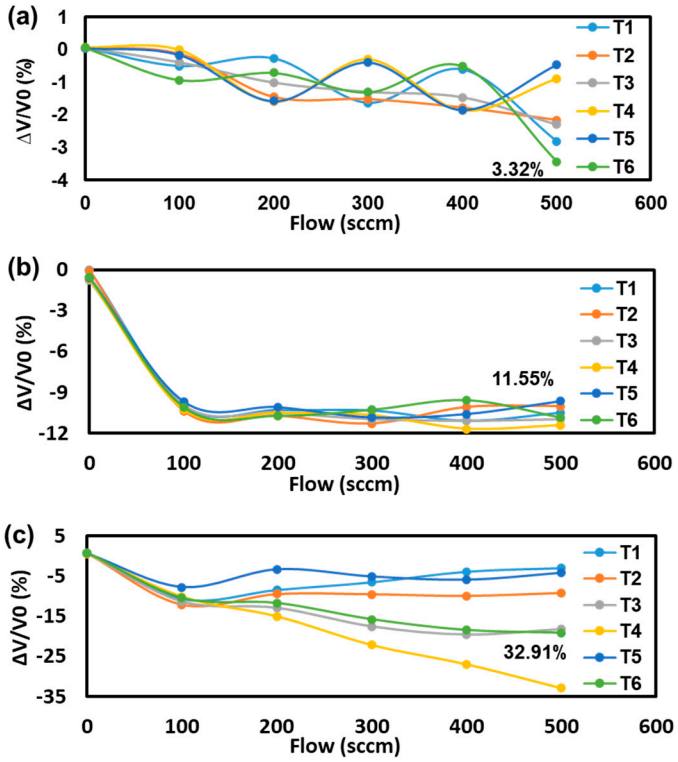

Figure 4. The ADT results of flow sensor with SSADT. (**a**) The maximum drift was 3.32% for 85℃; (**b**). The maximum drift was 11.55% for 120℃; (**c**). The maximum drift was 32.19% for 150℃.

To further analyzed the attenuation of SPS in MEMS flow sensor system. The SPS before and after the ADT test were calculated. As is shown in Table 3, taking the flow rate of 500 sccm as an example, ADT-C is the initial value of the MEMS flow chip and ADT-S is initial value of SPS. C-ADT is aging value of the MEMS flow chip and S-ADT is aging value of SPS. By comparison, it finds that the attenuation of SPS in ADT is significantly greater than that of the MEMS flow chip. The minimum drift of SPS accounts for 82.01% of this MEMS flow sensor system.

Table 3. The ADT Results of Flow Sensor and SPS

Index	#1	#2	#3	#4	#5	#6
ADT-C (mV)	9.533	9.752	9.634	9.607	9.611	9.664
C-ADT (mV)	9.529	9.751	9.621	9.603	9.591	9.657
Drift (%)	17.29	0.81	1.37	1.925	17.98	3.43
ADT-S (V)	4.801	4.856	4.894	4.893	4.893	4.816
S-ADT (V)	4.778	4.733	3.943	4.685	4.782	4.612
Drift (%)	82.70	99.19	98.63	98.07	82.01	96.56

3.2. Modelling Description

As is known, the resistance tends to produce a thermally drift, which is a function of time t and temperature T. Because there are thermal cycles in this SSADT, it is necessary to incorporate a Coffin-Manson component. The Coffin Manson model reflects the fatigue failure of products under thermal sequential stress, and has also been successfully used to simulate the crack propagation process of solder joints subjected to temperature impact [28–31]. Thus, it can be used to describe the relationship

Preprints (www.preprints.org) | NOT PEER-REVIEWED | Posted: 19 September 2023 doi:10.20944/preprints202309.1271.v1

between thermal fatigue failure and temperature cyclic stress of products. The resistance drift based on Coffin-Manson dependency had been proposed.

$$\frac{\Delta R}{R_0} = exp\left[-\frac{\Delta E}{K_B}\cdot\left(\frac{1}{T_1}-\frac{1}{T_2}\right)\right] \quad (2)$$

$$\varepsilon = \frac{A_0}{\Delta T^{\beta 1}} \cdot \frac{1}{f^{\beta 2}} \cdot exp\left[\frac{\Delta E}{K_B T_{max}}\right] \quad (3)$$

K_B is the Boltzmann's constant $8.36\times10^{-5}eV/^{\circ}K$. T_{max} is the maximum temperature. ΔE is activation energy of two different ADT stress. ΔR is drift. t is the time of ADT. T_1 and T_2 are different environmental temperature. ε is cycle-index. ΔT is operation temperature. f is cycle frequency. A_0, $\beta 1$, and $\beta 2$ is undetermined constant.

From Figure 3 and Figure 4, the drift rate could be calculated. For MEMS sensor chip, we could get the ΔE of assets with different stress via the drift. Furthermore, the drift of RHG was more stable with a maximum average drift rate in various assets groups. Consequently, the activation energy of each group tested assets could be acquired by calculating the RHG drift rate with different ADT conditions. Then, the activation energy of 85℃ ($\Delta E_{25℃-85℃}$), 120℃ ($\Delta E_{25℃-120℃}$) and 150℃ ($\Delta E_{25℃-150℃}$) of sensor chip were obtained by Equation (4) with the maximum average drift was 1.01%, 1.47% and 2.04%, respectively.

$$\Delta E_{(T_1-T_2)} = \frac{8.36\times10^{-5}eV/K \cdot ln\left(\frac{\Delta R_{RHG}}{R_{RHG0}}\right)}{\frac{1}{T_1}-\frac{1}{T_2}} \quad (4)$$

$$\Delta E_{25℃-85℃} = \frac{8.36\times10^{-5}eV/K\cdot ln\,(1.01)}{\frac{1}{298K}-\frac{1}{358K}} = 0.0015\ \text{eV}$$

$$\Delta E_{25℃-120℃} = \frac{8.36\times10^{-5}eV/K \cdot ln\,(1.47)}{\frac{1}{298K}-\frac{1}{393K}} = 0.039\ \text{eV}$$

$$\Delta E_{25℃-150℃} = \frac{8.36\times10^{-5}eV/K \cdot ln\,(2.04)}{\frac{1}{298K}-\frac{1}{423K}} = 0.060\ \text{eV}$$

Meanwhile, the parameter of Coffin-Manson is obtained with ΔE of SSADT. As shown in Table 4, the value is 2.303 for A_0, 0.154 for $\beta 1$, and 0.187 for $\beta 2$. Based on the above research, the ΔE of different SSADT of this flow sensor can be estimated without having to go to calculate the ΔR.

Table 4. The Parameter Estimation of Coffin-Manson Results of Flow Sensor Chip

Index	ε	f	$\Delta T(K)$	$T_{max}(K)$	ΔE(eV)	A_0	$\beta 1$	$\beta 2$
25℃ – 85℃	2	0.5	60	85	0.0015	2.303	0.154	0.187
25℃ – 120℃	2	0.5	95	120	0.039	2.303	0.154	0.187
25℃ – 150℃	2	0.5	125	150	0.060	2.303	0.154	0.187

Similarly, the E_a of this MEMS Flow sensor with different stress via the drift can be obtained. Thus, activation energy could be calculated with the maximum average drift was 1.21%, 11.15%, and 16.82%, respectively by flow rate was 500 sccm. Then, the activation energy of 85℃ ($\Delta E_{25℃-85℃}$), 120℃

Preprints (www.preprints.org) | NOT PEER-REVIEWED | Posted: 19 September 2023 doi:10.20944/preprints202309.1271.v1

($\Delta E_{25℃-120℃}$), and 150℃ ($\Delta E_{25℃-150℃}$) of Flow sensor were obtained by Equation (5) with the maximum activation energy was 0.028 eV, 0.359 eV, and 0.421 eV, respectively. At the same way, the parameter of Coffin-Manson of Flow sensor is obtained with ΔE of SSADT. As shown in Table 5, the value is 1.764 for A_0, 0.235 for $\beta 1$, and 0.298 for $\beta 2$, as shown in Table 5.

$$\Delta E_{25℃-85℃} = \frac{8.36\times10^{-5} eV/K \cdot ln\,(1.21)}{\frac{1}{298K}-\frac{1}{358K}} = 0.028 \text{ eV}$$

$$\Delta E_{25℃-120℃} = \frac{8.36\times10^{-5} eV/K \cdot ln\,(11.15)}{\frac{1}{298K}-\frac{1}{393K}} = 0.249 \text{ eV}$$

$$\Delta E_{25℃-150℃} = \frac{8.36\times10^{-5} eV/K \cdot ln\,(16.82)}{\frac{1}{298K}-\frac{1}{423K}} = 0.238 \text{ eV}$$

Table 5. The Parameter Estimation of Coffin-Manson Results of Flow Sensor

Index	ε	f	$\Delta T(K)$	$T_{max}(K)$	ΔE(eV)	A_0	$\beta 1$	$\beta 2$
25℃ – 85℃	2	0.5	60	85	0.028	1.764	0.235	0.298
25℃ – 120℃	2	0.5	95	120	0.249	1.764	0.235	0.298
25℃ – 150℃	2	0.5	125	150	0.238	1.764	0.235	0.298

According to the ΔE had obtained by the drifts and the lifetime would be estimated. And ε had obtained from Coffin-Manson modeling. Specifically, Arrhenius lifetime model is employed in the degradation model, which had been widely used in the reliability literature [31–34].

$$N_1 = \frac{l_1}{l_1'} = exp\left[\frac{\Delta E}{K_B}\cdot\left(\frac{1}{S1}-\frac{1}{S'}\right)\right] \quad (5)$$

N_1 is Arrhenius accelerator. l_1 is the lifetime of $S1$. l_1' is the lifetime of S'. The lifetime at various conditions could be estimated. For this MEMS flow sensor system, the lifetime was calculated, as shown in Table 6. It could be found that the lifetime shrunk more obviously from 8.290 years to 0.594 years in a range of 85℃ to 150℃. But for sensor chip, the change was 29.702 to 14.724 years. In addition, the lifetime of other conditions was acquired with obtained lifetime-stress data fitting. As is shown in Figure 5 (a) and (b), the predicted lifetime distributions are presented.

Preprints (www.preprints.org) | NOT PEER-REVIEWED | Posted: 19 September 2023 doi:10.20944/preprints202309.1271.v1

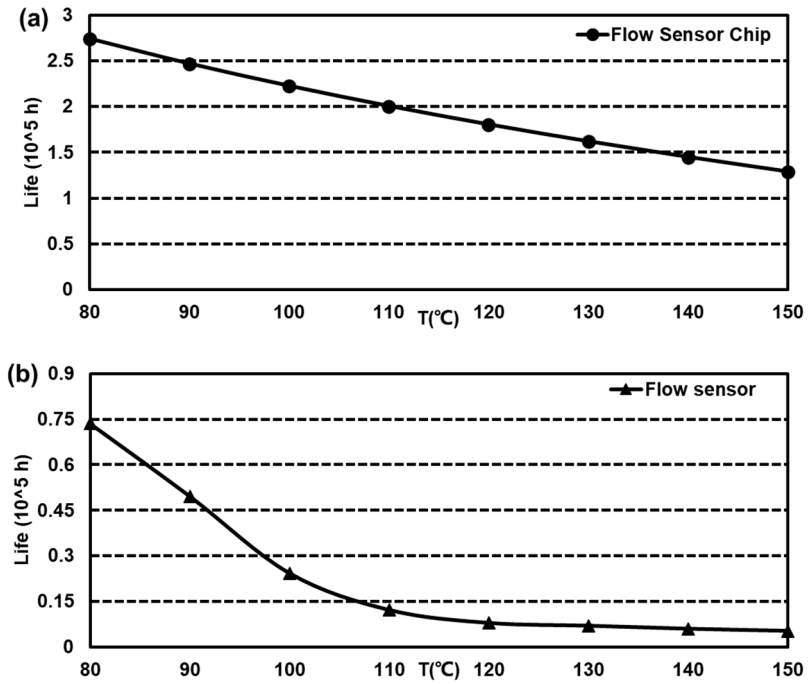

Figure 5. The ADT results of lifetime-stress. (a) The lifetime-stress of MEMS sensor chip; (b). The lifetime-stress of MEMS sensor.

Table 6. The Estimation of Lifetime

Index	Tem (℃)	E_a (eV)	Lifetime (years)
Sensor-chip-RHG	85℃	0.0015 eV	29.702
	120℃	0.039 eV	20.548
	150℃	0.060 eV	14.724
Flow sensor-500 sccm	85℃	0.028 eV	8.290
	120℃	0.249 eV	0.893
	150℃	0.238 eV	0.594

4. Reliability Description

Reliability engineering has become a powerful tool to determine the behavior of devices over time. One of the most ingrained concepts within reliability is the description of survival rate through the lifetime distribution modeling. For further exploring, it was necessary for us to evaluate the lifetime distribution. As we can see from the introduced publications, there are many methods for the description of lifetime distribution, Exponential distribution (ED), Weibull distribution (WD), Gamma, and Gaussian distribution [35–38]. Each lifetime distribution model contains a cumulative distribution function and a reliability function.

Considering numerous versions and types, we select the WD model to be a reliability model. On account of WD modifications have been proposed through diverse mathematical techniques to ensure that the behavior described is closest to the most of devices [39–41]. The cumulative distribution function F(t) and the reliability function R(t) could be calculated. The reliability-related parameters of the F(t) and R(t) are crucial adjective.

$$F(t) = 1 - \exp\left[-\left(\frac{t}{\alpha_0}\right)^{\beta}\right] \quad (6)$$

Preprints (www.preprints.org) | NOT PEER-REVIEWED | Posted: 19 September 2023 doi:10.20944/preprints202309.1271.v1

$$R(t) = \exp\left[-\left(\frac{t}{\alpha_0}\right)^{\beta}\right] \quad (7)$$

The α_0 is the scale factor or characteristic function. β is the shape factor or shape parameter. α_0 and β and could be obtained by fitting procedure [37–42]. t is working time.

After obtaining the modeling, the results were analyzed as shown in Figure 6 (a)- (c). The log time of accelerated was displayed in horizontal coordinate axis and the ln[-ln(1-F(t)] in the vertical. The results at each stress level were fit in straight lines. Therefore, it could be considered that the failure time of this Flow sensor was obeyed to WD under different temperature stresses. The R-squared of 85℃, 120℃, and 150℃ were displayed in Table 7. In addition, α_0, β, and the $R(t)$ were acquired, respectively, with 3000 hours aging time. As shown in Table 7, the $R(t)$ of this Flow sensor was 87.69% with 85℃. At the same time, the $R(t)$ was 32.77% for 120℃ and 19.39% for 150℃. Thus, the reliability of this Flow sensor with different T_s was acquired.

Table 7. The Parameter Estimation of Reliability

Index	85℃	120℃	150℃
α_0 $(\cdot 10^5)$	0.726	0.0781	0.0523
β	0.96	0.96	0.96
R(t)(%)	87.69	32.77	19.39

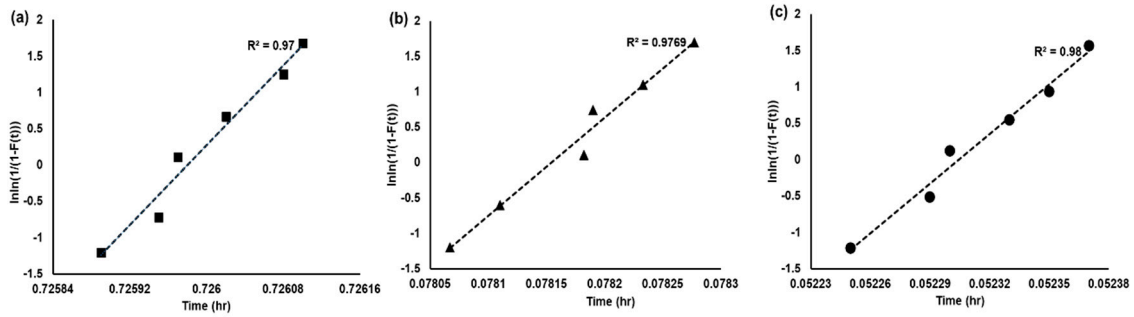

Figure 6. The fitting results of MEMS flow sensor with WD distribution. (**a**) The WD distribution result of 85℃; (**b**). The WD distribution result of 120℃; (**a**) The WD distribution result of180℃.

5. Conclusions

In this paper, the reliability of a MEMS flow sensor with T_s is estimated. The degradation characteristics of the MEMS flow sensor chip and the Flow sensor with SSADT are acquired. The biggest drift of 85℃, 120℃, and 150℃ are 1.35%, 2.09%, and 3.15% for the MEMS flow sensor chip. For flow sensor, the biggest drift is -32.91% at 500 sccm with 150℃. By analysis, it can be found that the attenuation of SPS is significant. The minimum drift of the signal processing system accounts for 82.01% of whole system. To obtain the lifetime of this flow sensor, the activation energy of 85℃,120℃, and 150℃ are calculated. The maximum activation energy is 0.028 eV, 0.359 eV, and 0.421 eV, respectively. By using the Coffin-Manson model, the relationship between cycle-index and T_s with SSADT is established. And the lifetime of MEMS flow sensor chip and flow sensor with different T_s is estimated by the Arrhenius. Furthermore, the reliability with WD is demonstrated. The $R(t)$ is 87.69% for 85℃, 32.77% for 120℃, and 19.39% for 150℃.

To sum up, the content illustrates the reliability study of a MEMS flow sensor with T_s. The results are innovative and original, and lay a foundation for this MEMS flow sensor to work under extreme temperature environment. Based on this research, the reliability database is set up. Moreover, we will further analysis the causes of degradation to instruct the design of this MEMS flow sensors system and make them more practical circumstances in complex conditions.

References

1. S. Wang, J. Wang, and X. Li, "Sensitivity Improvement of P + Si/Au Thermopile-Based Gas Flow Sensor by Optimizing Heat-Sink and Thermal-Insulation Configuration," in 2020 IEEE 33rd International Conference on Micro Electro Mechanical Systems (MEMS), 2020.
2. G. Kaltsas, A. A. Nassiopoulos, and A. G. Nassiopoulou, "Characterization of a silicon thermal gas-flow sensor with porous silicon thermal isolation," Sensors Journal IEEE, vol. 2, no. 5, pp. 463-475, 2015.
3. H. Sturm, G. Dumstorff, P. Busche, D. Westermann, and W. Lang, "Boundary Layer Separation and Reattachment Detection on Airfoils by Thermal Flow Sensors," Sensors (14248220), vol. 12, no. 11, pp. 14292-14306, 2012.
4. B. Fang, A. F. Lu, "The Simulation of Extremely Low Cycle Fatigue Fracture Behavior for Pipeline Steel (X70) Based on Continuum Damage Model," METALS, vol. 13, no. 7, pp. 825-829, 2023.
5. L. A. Escobar and W. Q. Meeker, "A review of accelerated test models," Statist. Sci., vol. 21, no. 4, pp. 552–577, 2006.
6. M. Hnommel, H. Knab, et al., "Electric properties of graphene-based conductive layers from DC up to terahertz range," Microelectronics Reliability, vol. 126, no. 6, pp. 1-6, 2021.
7. J. Heo, M. Park, "Effect of Flexible Operation on Residual Life of High-Temperature Components of Power Plants," PROCESSES, vol. 11, no. 6, pp. 1254–1266, 2023.
8. B. George, N. Muthuveerappan, "Life assessment of a high temperature probe designed for performance evaluation and health monitoring of an aero gas turbine engine," INTERNATIONAL JOURNAL OF TURBO & JET-ENGINES, vol. 40, no. 2, pp. 139-146, 2023.
9. Z. L. Wang, X. W. Cheng, et al., "Time-dependent concurrent reliability-based design optimization integrating experiment-based model validation," Structural and Multidisciplinary Optimization, vol. 01, no.1, pp.1314-1317, 2017.
10. Ali, S., Ali, S., Shah, I., & Khajavi, A. N, "Reliability analysis for electronic devices using beta generalized Weibull distribution," Iranian Journal of Science and Technology, Transactions A: Science, vol. 43(5), pp. 2501–2514, 2019.
11. V. A. Raghavan, B. Roggeman, M. Meilunas, et P. Borgesen, "Effects of 'latent damage' on pad cratering: reduction in life and a potential change in failure mode," Microelectron. Reliability, vol. 53, pp. 303–313, 2013.
12. E. Ben Romdhane, A. Gu´edon-Gracia, S. Pin, P. Roumanille, et H. Fr´emont, "Impact of crystalline orientation of lead-free solder joints on thermomechanical response and reliability of ball grid array components," Microelectron. Reliability, vol. 114, pp. 113812, 2020.
13. S. Limon, O. P. Yadav, and H. Liao, "A literature review on planning and analysis of accelerated testing for reliability assessment," Qual. Rel. Eng. Int, vol. 33, no. 8, pp. 2361–2383, 2017.
14. D. Shen, T. Liu, L. Zhang, et al., "A novel ADT design considering stress optimization," Clust. Comput, vol. 20, pp. 1–10, 2018.
15. L. A. Escobar and W. Q. Meeker, "A review of accelerated test models," Statist. Sci., vol. 21, no. 4, pp. 552–577, 2006.
16. C. J. Lu, W.Q. Meeker, et al., "Using degradation measures to estimate a time-to-failure distribution," Technometrics, vol. 35, no. 2, pp. 161–174, 1993.
17. S. J. Wu, C.T. Chang, et al., "Optimal design of degradation tests in presence of cost constraint," Reliab. Eng. Syst. Saf., vol. 76, no. 2, pp. 109–115, 2002.
18. Z. W. Wang, G. Liu, et al., "Electric properties of graphene-based conductive layers from DC up to terahertz range," Microelectronics Reliability, vol. 124, no. 4, pp. 1-9, 2021.
19. C. M. Liao, S.T. Tseng, et al., "A novel optimal accelerated degradation test design method considering multiple decision variables," IEEE Trans. Reliab., vol. 55, no. 1, pp. 59–66, 2016.
20. F. P. Cortes, E. Fabris, S. Bampi, "Analysis and design of amplifiers and comparators in CMOS 0.35 μm technology," Microelectronics Reliability, vol. 44, no. 4, pp. 657-664, 2004.
21. S. Jagtap, D. Sharma, S. Gupta, "Design of SET tolerant LC oscillators using distributed bias circuitry," Microelectronics Reliability, vol. 55, no. 9, pp.1537-1541, 2015.
22. D. Chiozzi, M. Bernardoni, N. Delmonte, P. Cova, "A simple 1-D finite elements approach to model the effect of PCB in electronic assemblies," Microelectronics Reliability, vol. 58, no. 26, pp. 126-132, 2016.
23. C. Chen, H. Hu, and J. J. Wang, "Numerical Study of the Thermal Thermopile Flow Sensor," in 2018 IEEE International Conference on Mechatronics and Automation (ICMA), 2018.

24. H. Zhou, P. Kropelnicki, J. M. Tsai, and C. Lee, "Development of a thermopile infrared sensor using stacked double polycrystalline silicon layers based on the CMOS process," Journal of Micromechanics & Microengineering, vol. 23, no. 6, p. 65026, 2013.
25. M. Dijkstra, T. Lammerink, M. Boer, R. J. Wiegerink, and M. Elwenspoek, "Ambient Temperature-Gradient Compensated Low-Drift Thermopile Flow Sensor," in IEEE International Conference on Micro Electro Mechanical Systems, 2009.
26. D. Randjelović, M. Frantlović, B. Miljković, B. Rosandić, Z. Jakšić, and B. Popović, "Intelligent Thermopile-Based Vacuum Sensor," Procedia Engineering, 2011.
27. D. V. Randjelović, B. Popović, P. Poljak, and O. Jaksic, "Sensing Gas Type and Pressure with Multipurpose Device Based on Seebeck Effect," in 2019 International Semiconductor Conference (CAS), 2019.
28. X. Q. Shi, et al., "Low cycle fatigue analysis of temperature and frequency effects in eutectic solder alloy," INTERNATIONAL JOURNAL OF FATIGUE, vol. 22, pp. 217-228, 2000.
29. Z. C. Ma, et al., "Modified Coffin-Manson equation to predict the fatigue life of structural materials subjected to mechanical-thermal coupling non-coaxial loading," JOURNAL OF MATERIALS SCIENCE & TECHNOLOGY, vol. 160, pp: 118-127, 2023.
30. L. J. Ding, et al., "Active Peltier Effect Heat Sink for Power Semiconductor Device Thermal Stability Enhancement," IEEE TRANSACTIONS ON POWER ELECTRONICS, vol. 38, pp: 11507-11520, 2023.
31. P. Roy, et al., "Reliability evaluation of carrier-based pulse width modulated three-level F-type neutral point clamped inverter with power loss analysis," INTERNATIONAL JOURNAL OF CIRCUIT THEORY AND APPLICATIONS, vol. 8, no. 1, pp. 1–9, 2023.
32. D. Liu and S. Wang, "Reliability estimation from lifetime testing data and degradation testing data with measurement error based on evidential variable and wiener process," Rel. Eng. Syst. Saf., vol. 205, 2021.
33. S. Limon, O. P. Yadav, and H. Liao, "A literature review on planning and analysis of accelerated testing for reliability assessment," Qual. Rel. Eng. Int., vol. 33, no. 8, pp. 2361–2383, 2017.
34. W. Q. Meeker, L. A. Escobar, and C. J. Lu, "Accelerated degradation tests: Modeling and analysis," Technometrics, vol. 40, no. 2, pp. 89–99, 1998.
35. Y. Ding, Q. Yang, C. B. King, and Y. Hong, "A general accelerated destructive degradation testing model for reliability analysis," IEEE Trans. Rel., vol. 68, no. 4, pp. 1272–1282, Dec. 2019.
36. Ali, S., Ali, S., Shah, I., Siddiqui, G. F., Saba, T., & Rehman, A, "Reliability analysis for electronic devices using generalized exponential distribution," IEEE Access, vol. 8, pp. 108629–108644, 2020.
37. D. B. Hani, AL. Athamneh, "Reliability modeling of the fatigue life of lead-free solder joints at different testing temperatures and load levels using the Arrhenius model," SCIENTIFIC REPORTS, vol. 13, no. 1, pp. 463–472, 2023.
38. B. Liu, Y. Teng, "A novel imprecise reliability prediction method for incomplete lifetime data based on two-parameter Weibull distribution. Proceedings of the Institution of Mechanical Engineers, Part O: Journal of Risk and Reliability," Technometrics, vol. 26, no. 2, pp: 157–171, 2018.
39. E. Bender, J. B. Bernstein, et al., "Reliability prediction of FinFET FPGAs by MTOL," Microelectronics Reliability, vol. 114, no. 3, pp: 1–6, 2020.
40. A. Acovic, G. L. Rosa, et al., "A review of hot-carrier degradation mechanisms in MOSFETs," Microelectronics Reliability, vol. 36, pp: 845-869, 1996.
41. J. Kohout, "Three-parameter Weibull distribution with upper limit applicable in reliability studies and materials testing," Microelectronics Reliability, vol. 137, pp. 1-10, 2022.